

ARTICLE

Structure, charge density, and Hirshfeld surface analysis of proton transfer complex 2-amino-4-methylpyridinium 2-(3-methylphenyl)-acetate

Chellam Anzline¹  | Samuel Israel¹  | Kanagasabapathi Sujatha² | Rajan Arul Jebamani Raja Sheeba¹

¹Department of Physics, The American college, Madurai, India

²Department of Physics, Erode Sengunthar Engineering College, Erode, India

Correspondence

Samuel Israel, Department of Physics, The American college, Madurai 625 002, India.
Email: israel.samuel@gmail.com

Abstract

The compounds m-Tolylacetic acid and 2-amino-4-Picoline were used as a precursor to synthesize the molecular complex 2-amino-4-methylpyridinium 2-(3-methylphenyl)-acetate by means of proton transfer. High-resolution X-ray diffraction data were collected for the crystallized complex at 100 K. The structure was solved spherically and further an aspherical model refinement was performed using Hansen and Coppens multipole formalism. Topological properties using AIM analysis were carried out for the title compound to understand the atom–atom interactions and the strength of the bond. The structure exhibits interesting patterns of N–H...O and C–H...O hydrogen bonds. A pair of N–H...O hydrogen bonds links the anion and cation of the molecular complex generating an $R^2_2(8)$ ring motif. These ring motifs are linked to adjacent anions and cations through another intermolecular N–H...O hydrogen bond generating a bifurcated $R^2_2(8)$ ring motif. Hirshfeld surface analysis was carried out to understand the types of inter-molecular interactions and their strengths.

KEYWORDS

AIM analysis, Hirshfeld surface analysis, multipole analysis, proton transfer

1 | INTRODUCTION

The determination of electronic distributions and associated properties from X-ray diffraction is a blossoming area in the field of crystallography. It was made known by W.H. Bragg that due to the periodic arrangement of atoms in crystals and the interaction of X-rays with the electrons in it, it is possible to understand the distribution of electron density from the intensity of the diffracted beams.^[1] This property was initially used to uncover the structure of crystals. The structure determination provides a lot of information like lattice parameters, geometrical parameters, addition of impurity atoms, and their contributions to lattice parameters. However, the physical, chemical, optical properties and the reactivity of the materials cannot be understood

from the structure information alone. Hence a unique tool called charge density distribution is preferred to completely understand the nature of the material.^[2]

The advent of new developments in experimental and computational techniques has made experimental charge densities to analyze a wide variety of problems in chemical interest. Such studies aid in understanding the features of chemical bonding in molecules from the topological analysis of electron densities^[3] and various electrostatic properties of molecules. Over the past three decades, charge density distribution of several materials like magnetic,^[4,5] energetic,^[6] NLO,^[7–11] and molecular complexes with biological properties have been reported.^[12,13] The effect of metal atoms in ligands has been analyzed using the topological properties of electron

density.^[14] In recent years, much attention has been paid to understanding the interaction of drug–receptor complex through charge density distribution.^[15–20] The structural knowledge of the active site at the electronic level helps to predict the interactive nature of the drug molecule. The electrophilic and nucleophilic sites of the molecule can be identified using the electrostatic potential map, which helps to confirm the reactive sites of the molecule.

In the present work, the charge density distribution of a molecular complex was studied, which was synthesized by utilizing proton transfer in *m*-Tolylacetic acid substituted pyridine molecular complex. The key intention of the present study is to determine the structure, charge density distribution, and the intermolecular interactions in the proton transfer complex 2-amino-4-methylpyridinium 2-(3-methylphenyl)-acetate. The crystal structure of the molecular complex was determined at low temperature (100 K) and the charge density distribution of the molecule was obtained from multipole analysis.^[21] AIM topological analysis of Bader was carried out to interpret the atom–atom interactions. An investigation of close intermolecular contacts through Hirshfeld surface analysis is also presented in order to quantify interactions within the crystal structure.^[22]

2 | CRYSTALLIZATION AND DATA COLLECTION

A mixture of 1 g of *m*-Tolylacetic acid and 0.72 g of 2-amino-4-Picoline is dissolved in 15 mL of acetone in an

equimolar ratio and it is kept at room temperature for slow evaporation. Tiny crystals suitable for taking X-ray diffraction were harvested after 15 days. A good quality single crystal was selected from the grown crystals for X-ray diffraction data collection for the charge density analysis. The complete data sets were collected from Bruker D8 CMOS PHOTON 100 single crystal X-ray diffractometer equipped with nitrogen cryostat apparatus. The diffraction data collection statistics are given in Table 1. The crystal structure of 2-amino-4-methylpyridinium 2-(3-methylphenyl)-acetate was solved by direct methods and refined by the full matrix least square technique on F^2 using SHELXL2014.^[23] Intensities were further scaled and corrected for absorption by SADABS.^[24] All H atoms clearly appear during the structure determination and their positions were stable during the refinement. The displacement ellipsoid atoms of the molecule generated from ORTEP3^[25,26] and PLATON^[27] routines incorporated in WINGX^[28] program are shown in Figure 1.

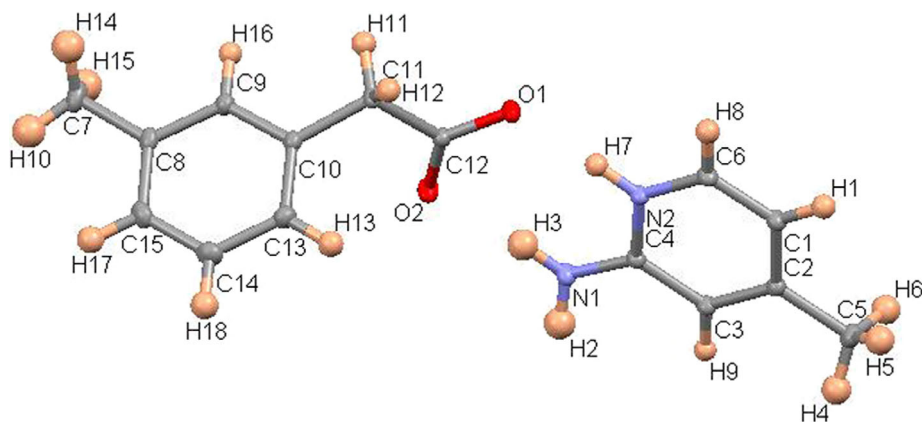
3 | MULTIPOLE ANALYSIS

The charge density analysis of 2-amino-4-methylpyridinium 2-(3-methylphenyl)-acetate was carried out using the crystallographic software MoPro^[29,30] where the Hansen and Coppens^[21] multipole formalism was incorporated for the determination of charge density of small as well as large molecules from the X-ray diffraction intensity data. According to Hansen and Coppens

TABLE 1 Crystal and data collection statistics

Chemical formula	C ₆ H ₉ N ₂ ⁺ .C ₉ H ₉ O ₂ ⁻
Molecular weight (g/Mol)	258.31
F(000)	276
Crystal system, space group	Triclinic, $P\bar{1}$
Temperature (K)	100 (1)
a, b, c (Å)	8.339(5), 9.338(6), 9.414(5)
α, β, γ (°)	85.259(14), 78.812(13), 71.030(15)
Volume (Å ³)	679.9(7)
Z	2
Radiation type	Mo K α (0.71073 Å)
μ (mm ⁻¹)	0.085
No. of measured reflections	141,738
No. of independent reflections	10,330
No. of observed reflections ($I > 2\sigma I$)	7,338
Index ranges	$-16 \leq h \leq +16, -18 \leq k \leq +18, -18 \leq l \leq +18,$
$\sin \theta/\lambda$ (Å ⁻¹)	1.02
Spherical atom model: R(F), wR(F ²), GoF	0.065, 0.237, 1.175
Multipole model refinement: R(F), wR(F ²), GoF	0.033, 0.059, 1.657

FIGURE 1 ORTEP view of the molecule showing the atom numbering scheme. Displacement ellipsoids are drawn with 50% probability level and hydrogen atoms are drawn as small circles



multipole formalism, the electron density of an atom is partitioned as follows:

$$\rho_{\text{atom}}(\mathbf{r}) = P_c \rho_{\text{core}}(\mathbf{r}) + P_v \kappa^3 \rho_{\text{val}}(\kappa \mathbf{r}) + \sum_{l=0, l_{\text{max}}} \kappa'^3 R_l(\kappa' \mathbf{r}) m_l \leq 1 \sum P_{lm} Y_{lm}(\theta, \varphi)$$

Here the total density is decomposed into core and valence electrons. The term ρ_{core} represents the spherically symmetric Hartree–Fock core electron density and ρ_{val} the spherically averaged free atom Hartree–Fock valence electron density. The form factors of the core ρ_{core} and of the spherical valence $\rho_{\text{val}}(\kappa \mathbf{r})$ can be computed from Clementi and Raimondi^[31] wave functions. The third term represents the nonspherical part of the electron density as a multipole density. The term Y_{lm} describes the spherical harmonic functions in real form. The radial functions $R_l(\mathbf{r})$ used here are of Slater type: $R_l(r) = r^{nl} \exp(-\kappa' \xi r)$ and can be obtained from Clementi wave functions. The charge density parameters P_c , P_v , P_{lm} and κ , κ' can be directly obtained from least square refinement and the kappa coefficients describe the expansion/contraction of the spherical and multipolar part of valence density.

The standard refinement procedure of MoPro was employed to perform the multipolar refinements. Initially, scale factor, xyz and Uij parameters were refined together and then κ , κ' , valence and multipole populations were refined successively. xyz and Uij parameters of all the non-H atoms were refined initially using all reflections and then high-order reflections to ensure the deconvolution of the thermal motion from the deformation electron density.^[32] Later these parameters were refined using all reflections. Then, the charge density parameters κ , κ' , P_{val} , and P_{lm} were refined successively. In the last cycles of the refinement, all parameters were refined together until convergence. During the refinement, the electron neutrality constraint was applied. Hexadecapole level ($l_{\text{max}} = 4$) of multipole expansion was used for the refinement of oxygen and

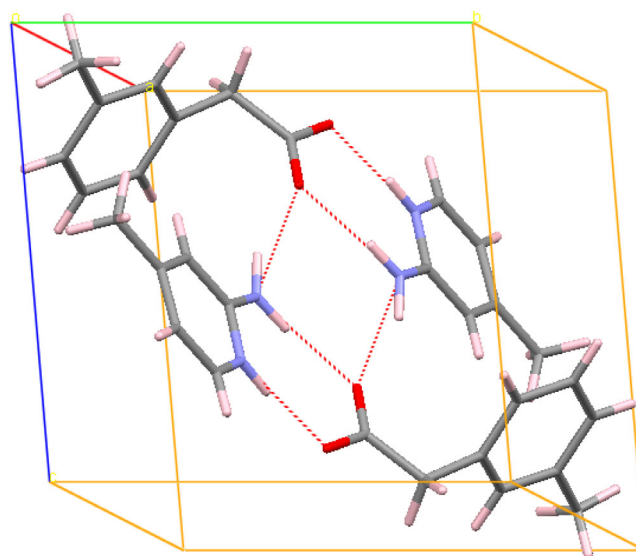


FIGURE 2 Crystal packing of the molecular salt along the a-axis showing the ring graph set motifs. Hydrogen bonding interactions are shown by dashed lines

nitrogen atoms, while carbon atoms were refined up to Octupole level ($l_{\text{max}} = 3$). To check the accuracy of the maps, deformation density maps were generated using VMoPro, which is the interactive visualization complement of MoPro package, which allows easy computation and graphical representation of the electron density maps and the derived molecular properties.^[29,30]

4 | RESULTS AND DISCUSSIONS

4.1 | Molecular structure

The molecular and crystal structures of 2-amino-4-methylpyridinium 2-(3-methylphenyl)-acetate have already been reported by Sivakumar et al.^[33] In the present study, a similar procedure proposed by Sivakumar et al. was adopted for the growth of the title molecule,

TABLE 2 Bond length and bond angle of the title molecule

<i>Bond length (Å)</i>					
O1-C12	1.267 (13)	C11-H11	0.995 (10)	N2-C6	1.358 (14)
O2-C12	1.248 (10)	C11-C12	1.527 (16)	C1-H1	1.009 (12)
C7-H10	0.963 (12)	C13-H13	1.002 (11)	C1-C2	1.418 (13)
C7-H15	0.962 (9)	C13-C14	1.387 (17)	C1-C6	1.356 (17)
C7-H14	0.976 (13)	C14-H18	0.971 (9)	C2-C3	1.365 (15)
C7-C8	1.503 (19)	C14-C15	1.385 (19)	C2-C5	1.503 (2)
C8-C9	1.404 (16)	C15-H17	1.004 (10)	C3-H9	0.980 (12)
C8-C15	1.380 (14)	N1-H3	0.883 (11)	C3-C4	1.414 (16)
C9-H16	0.973 (8)	N1-H2	0.861(12)	C5-H4	0.891 (17)
C9-C10	1.384 (16)	N1-C4	1.331(14)	C5-H5	0.872 (16)
C10-C11	1.502 (16)	N2-H7	0.885 (13)	C5-H6	0.897 (16)
C10-C13	1.394 (13)	N2-C4	1.355 (11)	C6-H8	0.966 (9)
C11-H12	1.000 (8)				
<i>Bond angle (°)</i>					
H1-C1-C6	120.3	N2-C6-C1	120.7	C10-C11-C12	116.9
H1-C1-C2	120.4	H10-C7-H14	109.4	O2-C12-O1	124.7
C6-C1-C2	119.2	H10-C7-H15	109.4	O2-C12-C11	119.8
C3-C2-C1	119.0	H10-C7-C8	109.4	O1-C12-C11	115.4
C3-C2-C5	120.8	H14-C7-H15	109.4	H13-C13-C14	119.8
C1-C2-C5	120.0	H14-C7-C8	109.4	H13-C13-C10	119.8
H9-C3-C2	119.9	H15-C7-C8	109.4	C14-C13-C10	120.2
H9-C3-C4	119.8	C15-C8-C9	118.4	H18-C14-C13	119.9
C2-C3-C4	120.2	C15-C8-C7	121.5	H18-C14-C15	120.0
N1-C4-N2	118.2	C9-C8-C7	119.9	C13-C14-C15	120.0
N1-C4-C3	123.1	H16-C9-C10	119.1	H17-C15-C8	119.6
N2-C4-C3	118.5	H16-C9-C8	119.1	H17-C15-C14	119.6
H6-C5-H4	109.4	C10-C9-C8	121.7	C8-C15-C14	120.7
H6-C5-H5	109.4	C9-C10-C13	118.8	H2-N1-H3	120.1
H6-C5-C2	109.4	C9-C10-C11	120.1	H2-N1-C4	118.0
H4-C5-H5	109.4	C13-C10-C11	120.8	H3-N1-C4	118.3
H4-C5-H5	109.4	H12-C11-H11	107.2	H7-N2-C4	118.9
H4-C5-C2	109.4	H12-C11-C10	108.0	H7-N2-C6	118.9
H5-C5-C2	109.4	H12-C11-C12	108.0	C4-N2-C6	122.1
H8-C6-N2	119.6	H11-C11-C10	108.0		
H8-C6-C1	119.6	H11-C11-C12	108.0		

and the structure was redetermined from low temperature (100 K) X-ray diffraction intensity measurements for charge density studies. Figure 1 consists of an anion and a cation where the cation, 2-amino-4-methylpyridinium is protonated at the pyridine N atom and the anion, 2-(3-methylphenyl)-acetate is deprotonated at hydroxy O atom. Figure 2 shows the molecular packing diagram of the molecule, which encloses two molecules within a unit cell, and the hydrogen bonding intermolecular interactions are shown by dashed lines. The bond lengths and

bond angles obtained after the structure refinement are listed in Table 2. The C–C bond lengths obtained after the refinement ranges from 1.380 to 1.404 Å, which is very close to the standard value of 1.39 Å. Among all the C–C atoms in the phenyl ring, C8–C15 has a slightly lower bond length than the C8–C9 bond, which may be due to the attachment of methyl group in C8. But in the pyridine ring, the bond length between C2–C3 and C6–C1 is 1.365 and 1.356 Å, while C3–C4 and C1–C2 has a bond length of 1.414 and 1.418 Å, which shows that

FIGURE 3 Three-dimensional view of static multipole deformation map

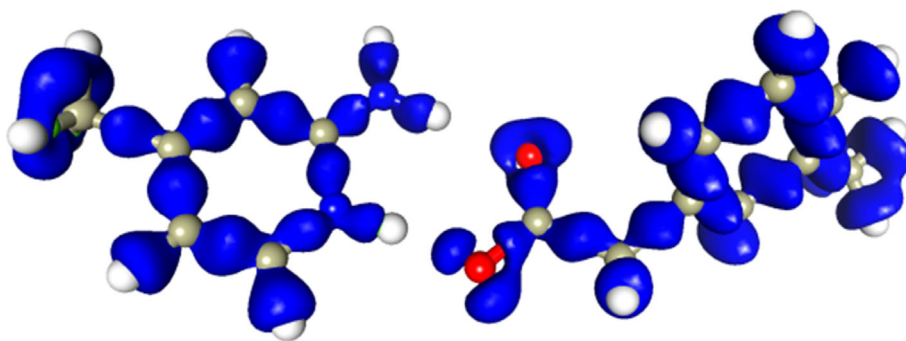
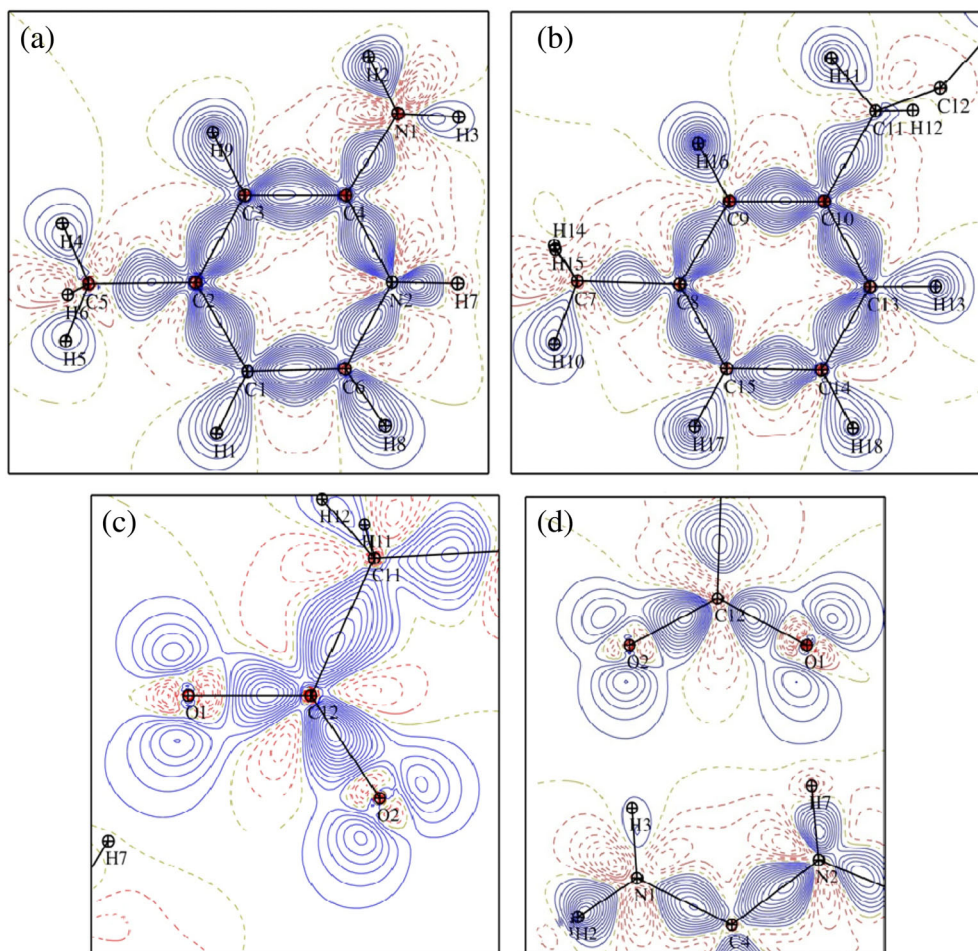


FIGURE 4 Static multipole deformation map of (a) C3–C4–N2 plane (pyridine ring) (b) C9–C10–C13 plane (phenyl ring) (c) O1–C12–O2 plane (d) O2–O1–H7 plane with a contour level of $0.05 \text{ e}\text{\AA}^{-3}$



pyridine has a conjugated system of π electrons that are delocalized over the ring. Other C–C atoms that do not lie in the ring have C–C values ranging from 1.501 to 1.527 Å that confirms the single bond nature of C7–C8, C10–C11, C11–C12, and C2–C5 bonds.^[34] The bond lengths for C–N and C–O lie in the range of 1.331–1.358 Å and 1.248–1.267 Å, which reveals that the bonding between C–N and C–O has double bond nature and the bond is strongly polarized toward the nitrogen and oxygen atom because of the high electronegativity of these atoms.^[35]

4.2 | Topological analysis of electron density

Static deformation density map is an important function derived from the multipole model, which represents the electron density in the bonding region of the molecule. The three-dimensional static deformation density map of the title molecule is depicted in Figure 3, which shows the accumulation of charges, the shape of the bonding regions, and the lone pair positions of the O atoms. The cross-sectional views of the same at different planes are

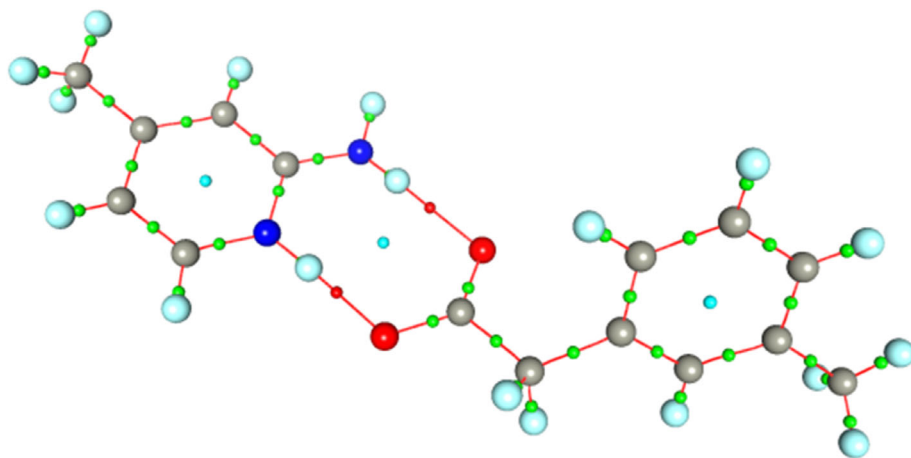


FIGURE 5 Molecular graph of 2-amino-4-methylpyridinium 2-(3-methylphenyl) acetate. Green dots represent the (3,−1) bond critical points

plotted in Figure 4, to visualize the interactions clearly. Figure 4a–d shows the deformation density map of C3–C4–N2 plane (pyridine ring), C9–C10–C13 plane (Phenyl ring), O1–C12–O2 plane and O2–O1–H7 plane with a contour level of $0.05 \text{ e}\text{\AA}^{-3}$. The interaction between C–C and C–N in the pyridine ring and the interaction of C–C in phenyl ring can be visualized from Figure 4a,b, which shows the shared shell interaction between C–C and C–N atoms. The electron lone pairs of O1 and O2 atoms are clearly visible in the deformation electron density map of O1–C12–O2 plane (Figure 4c) and the noncovalent interaction between O1–H7 and O2–H3 can be visualized from Figure 4d.

A critical point search has been carried out in all bonds of the molecule, and a (3,−1) type critical point namely a bond critical point was found, which confirms that the bonds in the molecule exhibit covalent interactions. Figure 5 shows the molecular graph of 2-amino-4-methylpyridinium 2-(3-methylphenyl)-acetate molecule showing the positions of bond critical points in the molecule. The topological properties of the electron density of the molecule have been calculated and are listed in Table 3. The electron density $\rho_{\text{BCP}}(r)$ of the C–C bonds on the phenyl ring of anion ranges from 2.022 to $2.132 \text{ e}\text{\AA}^{-3}$ while other C–C bonds in the anion have the value of $\rho_{\text{BCP}}(r)$ that ranges from 1.654 to $1.673 \text{ e}\text{\AA}^{-3}$. The high density of C–C bonds in the phenyl ring reveals the delocalization of electrons and the other C–C bonds in the anion has a slightly lower density, which confirms the bonding as single bond. Similar behavior was observed in the cation. The C–C bonds in the pyridine ring of cation have $\rho_{\text{BCP}}(r)$, which ranges from 2.043 to $2.140 \text{ e}\text{\AA}^{-3}$, while C2–C5 bond has a density of $1.688 \text{ e}\text{\AA}^{-3}$. This shows the delocalization of electrons in pyridine ring and a strong interaction between C–C bonds of the pyridine ring and a little weak interaction in C2–C5. The interaction between C–H bonds in anion ranges from 1.673 to

$1.836 \text{ e}\text{\AA}^{-3}$, while in the cation, it ranges from 1.684 to $1.924 \text{ e}\text{\AA}^{-3}$. The two C–N bonds in the cation has the density of 2.262, $2.296 \text{ e}\text{\AA}^{-3}$, which shows that the interaction between C–N is slightly greater than C–C. Also, the N–H bond in the pyridine ring has little lower density than the N–H bonds in the amino group. In the molecular complex, C–O bond has the highest density among all other bonds, which indicates the double bond nature of C–O and the analysis reveals $\rho_{\text{BCP}}(\text{O2-C12}) > \rho_{\text{BCP}}(\text{O1-C12})$. The above analysis also confirms that the CP in the heteronuclear C–O, C–N, C–H, and N–H bonds is always located closer to the less electronegative atom.^[36] This is evident from the d_1 and d_2 values of (3,−1) critical points and it is shown in Table 3. The polarization effect in C–H and N–H bonds is predominantly higher compared with the non-hydrogen bonds. This difference is due to the heavy and light atom interaction.^[35]

4.3 | Gradient vector field

The gradient vector field of electron density of 2-amino-4-methylpyridinium 2-(3-methylphenyl)-acetate molecule was plotted using WINXPRO program.^[37] Figure 6a,b shows the charge density gradient trajectories in C3–C4–N2 and O1–C12–O2 plane. The gradient trajectories are originated at the atomic centers and terminate at the bond critical point. The volume of N1 and N2 is high compared with all C atoms, whereas the oxygen atoms O1 and O2 exhibit a very large volume compared with the other atoms present in the molecule. The atomic basins of carbon and nitrogen atoms have a prismatic form while oxygen and hydrogen atoms are drop shaped. In both the figures, the gradient lines are dominant in the core of the atomic basin of all atoms and it decreases as the distance from the nucleus increases. This is due to the asphericity of the valence electron density.^[38]

TABLE 3 Topological properties of (3,−1) bond critical points

Bond (A1-A2)	d (Å)	d ₁ (A1-CP) (Å)	d ₂ (CP-A2) (Å)	ρ (eÅ ⁻³)	∇ ² ρ (eÅ ⁻⁵)	λ ₁ (eÅ ⁻⁵)	λ ₂ (eÅ ⁻⁵)	λ ₃ (eÅ ⁻⁵)	ε
O1-C12	1.265	0.796	0.469	2.512	−32.79	−23.55	−21.91	12.67	0.074
O2-C12	1.252	0.786	0.466	2.748	−37.8	−27.32	−23.96	13.48	0.140
N1-H3	1.010	0.697	0.313	2.256	−37.98	−36.87	−34.9	33.78	0.056
N1-H2	1.010	0.677	0.333	2.459	−36.34	−34.72	−31.78	30.17	0.092
N1-C4	1.336	0.767	0.569	2.262	−22.8	−18.74	−16.19	12.14	0.157
N2-H7	1.010	0.769	0.241	1.888	−31.28	−31.77	−30.3	30.79	0.048
N2-C4	1.352	0.806	0.546	2.296	−24.99	−19.25	−16.59	10.85	0.120
N2-C6	1.357	0.801	0.556	2.166	−22.5	−17.42	−16.24	11.16	0.072
C1-H1	1.080	0.683	0.397	1.881	−20.68	−18.88	−17.6	15.8	0.072
C1-C2	1.419	0.682	0.737	2.076	−19.03	−16.17	−13.52	10.66	0.196
C1-C6	1.368	0.687	0.681	2.203	−21	−17.22	−14.1	10.33	0.220
C2-C3	1.377	0.720	0.657	2.140	−19.86	−16.77	−13.8	10.7	0.215
C2-C5	1.499	0.788	0.711	1.688	−13.42	−11.54	−10.76	8.89	0.072
C3-H9	1.080	0.681	0.399	1.873	−19.01	−18.14	−16.84	15.97	0.077
C3-C4	1.415	0.721	0.694	2.043	−17.48	−15.7	−13.36	11.59	0.175
C5-H4	1.080	0.684	0.326	1.781	−16.78	−16.27	−12.03	11.52	0.352
C5-H5	1.080	0.685	0.395	1.684	−15.22	−14.39	−10.35	9.51	0.389
C5-H6	1.080	0.688	0.392	1.687	−17.2	−16.09	−11.93	10.81	0.349
C6-H8	1.080	0.686	0.394	1.924	−20.36	−20.54	−19.17	19.35	0.071
C7-H10	1.080	0.682	0.398	1.742	−15.53	−15.84	−14.32	14.63	0.106
C7-H15	1.080	0.689	0.391	1.700	−14.63	−14.42	−11.69	11.48	0.233
C7-H14	1.080	0.683	0.397	1.748	−15.88	−15.87	−13.7	13.69	0.158
C7-C8	1.505	0.744	0.760	1.654	−11.9	−11.24	−10.62	9.96	0.058
C8-C9	1.398	0.756	0.642	2.050	−19.09	−15.32	−12.58	8.82	0.217
C8-C15	1.392	0.720	0.672	2.132	−20.75	−16.74	−13.65	9.64	0.226
C9-H16	1.080	0.691	0.389	1.836	−18.16	−16.1	−14.72	12.66	0.093
C9-C10	1.392	0.659	0.733	2.079	−19.07	−15.68	−12.47	9.08	0.257
C10-C11	1.503	0.782	0.721	1.663	−10.78	−11.17	−10.74	11.13	0.039
C10-C13	1.399	0.688	0.711	2.118	−20.28	−17.09	−13.66	10.46	0.251
C11-H12	1.080	0.698	0.382	1.704	−13.83	−15.03	−12.7	13.91	0.183
C11-H11	1.080	0.685	0.395	1.712	−13.36	−15.49	−15.2	17.34	0.019
C11-C12	1.528	0.737	0.791	1.673	−11.14	−12.03	−10.62	11.51	0.132
C13-H13	0.962	0.671	0.291	1.791	−17.83	−17.11	−16.81	16.1	0.018
C13-C14	1.390	0.733	0.657	2.059	−18.12	−15.48	−13.18	10.54	0.174
C14-H18	1.080	0.696	0.384	1.809	−18.26	−17.22	−16.47	15.42	0.045
C14-C15	1.396	0.707	0.689	2.022	−16.83	−15.04	−12.45	10.66	0.207
C15-H17	1.080	0.688	0.392	1.768	−16.01	−15.99	−14.79	14.77	0.081

4.4 | Laplacian of the electron density

The second derivative of electron density $\rho_{\text{BCP}}(r)$ is the Laplacian of the electron density $\nabla^2\rho_{\text{BCP}}(r)$, which gives information about the nature of chemical bonding in the

molecule. If the Laplacian of electron density $\nabla^2\rho_{\text{BCP}}(r) < 0$, the charges are locally concentrated and the interaction is termed as open shell, whereas if $\nabla^2\rho_{\text{BCP}}(r) > 0$, the charges are locally depleted, which indicates that the interaction is closed shell type.

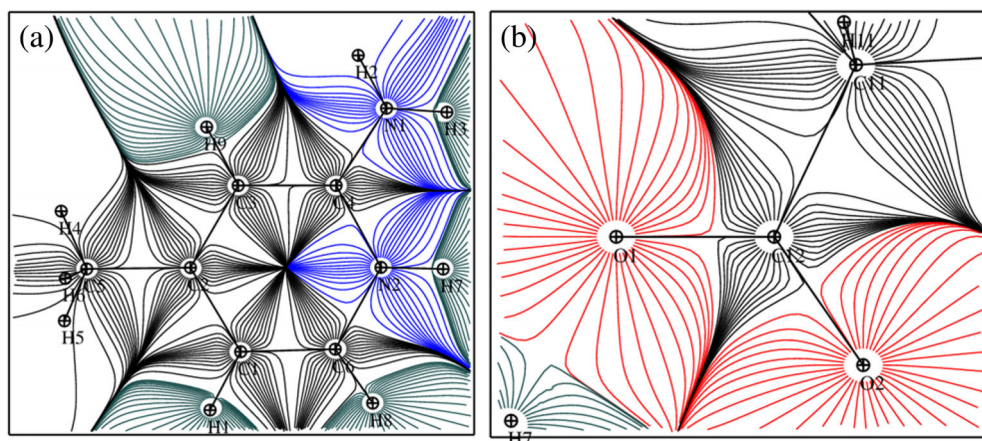


FIGURE 6 Gradient map of (a) C3-C4-N2 plane (b) O1-C12-O2 plane

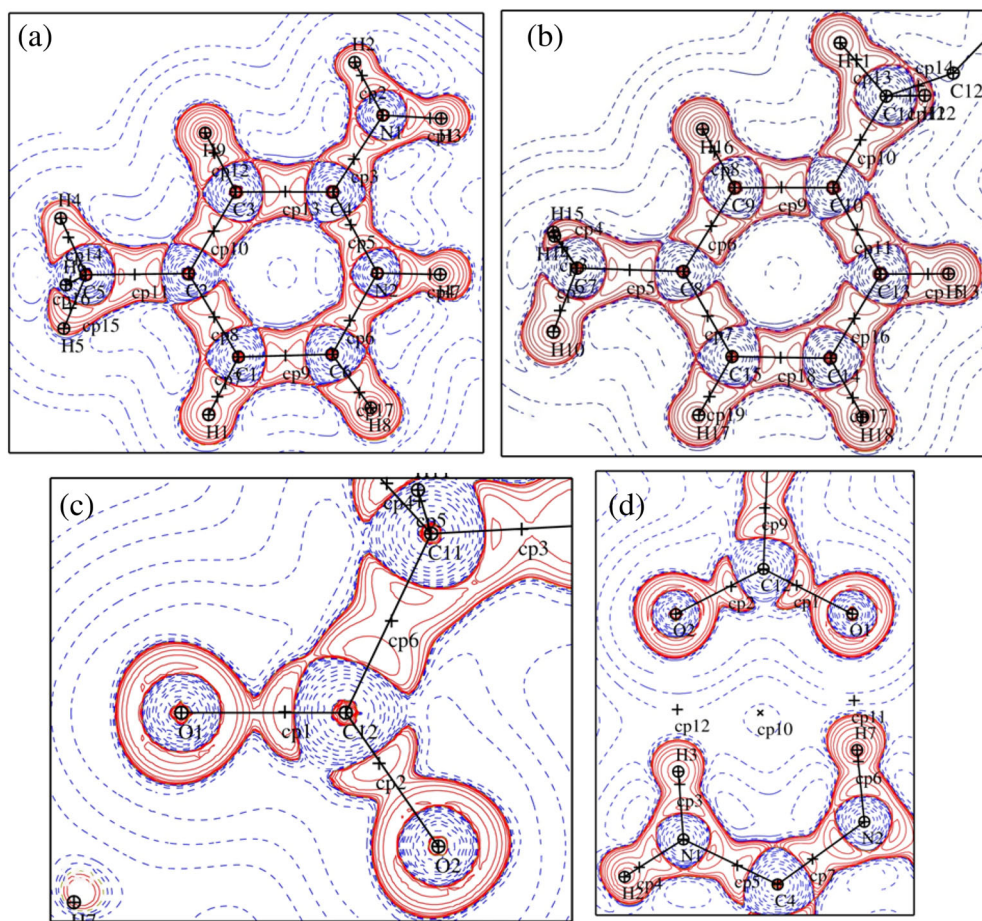


FIGURE 7 Laplacian map of (a) C3-C4-N2 plane (pyridine ring) (b) C9-C10-C13 plane (phenyl ring) (c) O1-C12-O2 plane (d) O2-O1-H7 plane. Blue and red lines represent the positive and negative contours

In the present analysis, all interactions have negative Laplacian with $\rho_{BCP}(r)$ ranging from 1.654 to 2.748 $\text{e}\text{\AA}^{-3}$, which shows that all the interactions are shared shell. As discussed in the previous section, the charge accumulation is not same for all $(C-C)_{\text{phenyl}}$ and $(C-C)_{\text{pyridine}}$ bonds of aromatic ring. A similar trend was observed in the Laplacian of electron density distribution. The Laplacian values of $(C-C)_{\text{phenyl}}(\text{ring})$ range from -16.83 to $-20.75 \text{ e}\text{\AA}^{-5}$, while other C-C atoms in anion have the Laplacian of -10.78 to $-11.9 \text{ e}\text{\AA}^{-5}$. Likewise, Laplacian

of $(C-C)_{\text{pyridine}}(\text{ring})$ bonds ranges from -17.48 to $-21.0 \text{ e}\text{\AA}^{-5}$. The above observation from anion and cation reveals that the charges are highly concentrated between the C-C bonds in the ring than other C-C bonds. The Laplacian of the N-H bonds ranges from $-31.28 \text{ e}\text{\AA}^{-5}$ to $-37.98 \text{ e}\text{\AA}^{-5}$, which is comparatively very high and it clearly indicates that the charges of the bond are highly concentrated compared with all other bonds in the molecule.^[39] For the X-H bonds (X = C, N), the magnitude of Laplacian increases as the X atom changes from C to

FIGURE 8 Isosurface representation of molecular electrostatic potential map of the title molecule. The positive (blue) surface is $0.9 \text{ e}\text{\AA}^{-1}$ and the negative (red) surface is $-0.04 \text{ e}\text{\AA}^{-1}$

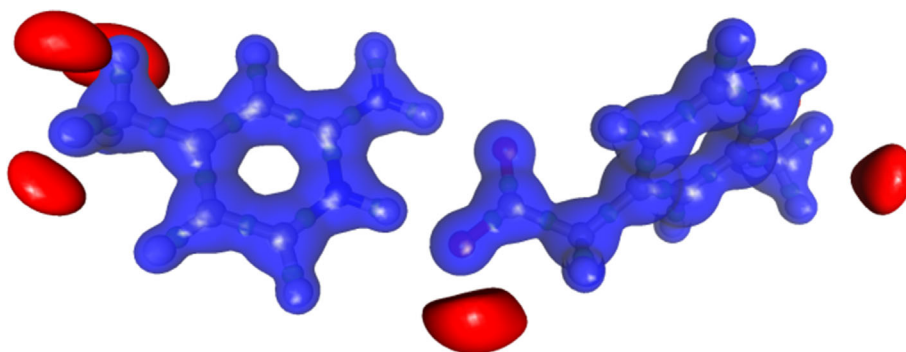


FIGURE 9 Hydrogen bonding network of the molecule showing N-H...O and C-H...O type of interaction

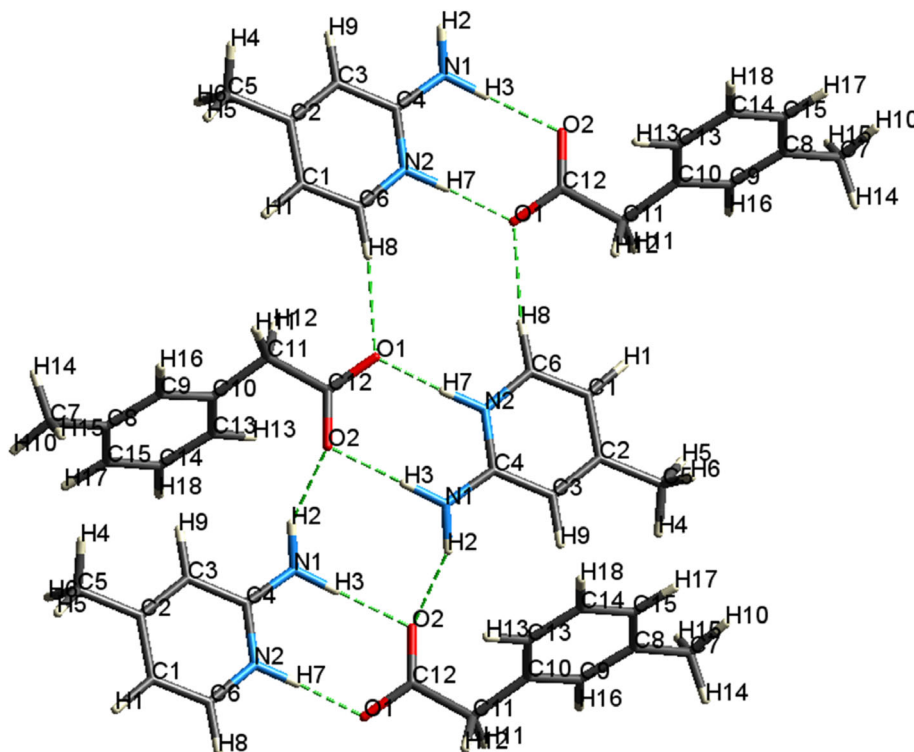


TABLE 4 Hydrogen bonding geometry

D-H...A	D-H (Å)	H...A (Å)	D-A (Å)	A-H...D (°)
N2-H7...O1	0.88 (7)	1.630 (13)	2.510 (12)	167.6
N1-H3...O2	0.88 (3)	1.850 (11)	2.730 (14)	170.8
N1-H2...O2 ⁽ⁱ⁾	0.86 (8)	1.881 (7)	2.741 (10)	153.1
C6-H8...O1 ⁽ⁱⁱ⁾	0.96 (9)	2.233 (6)	3.193 (11)	169.8

Note: (i) x, y, z; (ii) -x, -y, -z.

N,^[40] which can be evident from Table 3. The spatial distribution of Laplacian map along the pyridine ring, phenyl ring, O1-C12-O2 plane O2-O1-H7 plane is shown in Figure 7. The shared shell or covalent interactions between C-C, C-N, and C-H bonds were clearly seen in the Laplacian of pyridine and phenyl ring. The charge concentration of all the C atoms and the N atom is clearly

triangular in shape, indicating a sp^2 -type C and N atom. Figure 7c clearly depicts the two lone pair electron lobes at O1 and O2 and it also reveals that the interaction between C and O is a shared shell. In Figure 7d, the critical points cp11 and cp12 between O1...H7 and O2...H3 show the noncovalent interaction between the anion and cation. The Laplacian map of O1-C12-O2 plane shows

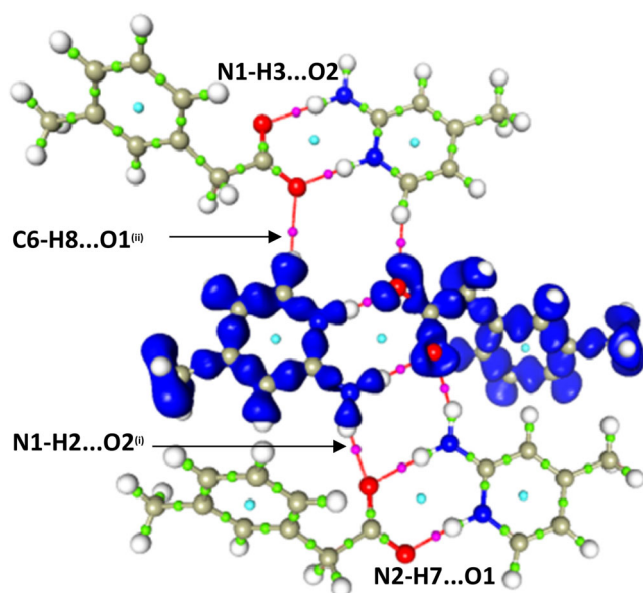


FIGURE 10 Molecular graph of intermolecular interactions. Green dots represent the (3,−1) bond critical points of shared shell interaction between atoms while the magenta dots indicate the (3,−1) bond critical points of intermolecular interactions

an almost spherical distribution around oxygen atoms, which indicates an even distribution of electrons, whereas other atoms have more deformation in the valence region than in the core region.

4.5 | Electrostatic potential

The electrostatic potential (ESP) has been calculated by using the electron density at the nuclear positions using the equation $\phi'(r) = \sum (Z_N/R_N - r') - \int (\rho(r)/|r - r'|) dr$ where Z_N is the charge^N of the nucleus N located at the position R_N .^[41] The ESP map provides information about the drug–receptor interaction, molecular recognition, and the chemical reactivity of the molecule.^[42] It also paves the way to identify the region of electrophilic and nucleophilic attack that sits in the molecule where the chemical reaction is expected to happen. The ESP map of 2-amino-4-methylpyridinium 2-(3-methylphenyl)-acetate molecule

has been generated using the method of Su and Coppens.^[43] Figure 8 displays the electrostatic potential surface of the title molecule where negative region represents the region of negative electrostatic potential, and the blue region shows the region of positive electrostatic potential.

4.6 | Hydrogen bond analysis and intermolecular interactions

The structure of the title molecule is stabilized by strong as well as weak intermolecular interactions in the crystal. Figure 9 shows the intermolecular interactions of the molecule in which the molecule forms N–H...O or C–H...O types of interactions with the neighboring molecules. The anion and cation of the proton transfer complex are linked by N2–H7...O1 and N1–H3...O2 intermolecular hydrogen bonds generating an $R^2_2(8)$ ring motif. These ring motifs are connected with adjacent anions and cations through N1–H2...O2 hydrogen bonds generating a bifurcated $R^2_2(8)$ ring motif. The intermolecular C6–H8...O1 and π – π interactions lead to the formation of three-dimensional network. The unique hydrogen bonding patterns observed in the crystal structure are shown in Figure 9. The hydrogen bonding parameters of N1–H2...O2⁽ⁱ⁾ are: N1...O2⁽ⁱ⁾ 2.741 Å, H2...O2⁽ⁱ⁾ 1.881 Å and for C6–H8...O1⁽ⁱⁱ⁾ are: C6...O1 3.193 Å, H8...O1⁽ⁱⁱ⁾ 2.233 Å where the symmetry codes are (i) x,y,z and (ii)–x,–y,–z. Similarly, the hydrogen bonds connecting the proton transfer complex are also listed in Table 4.

4.7 | Topology of hydrogen bonded interactions

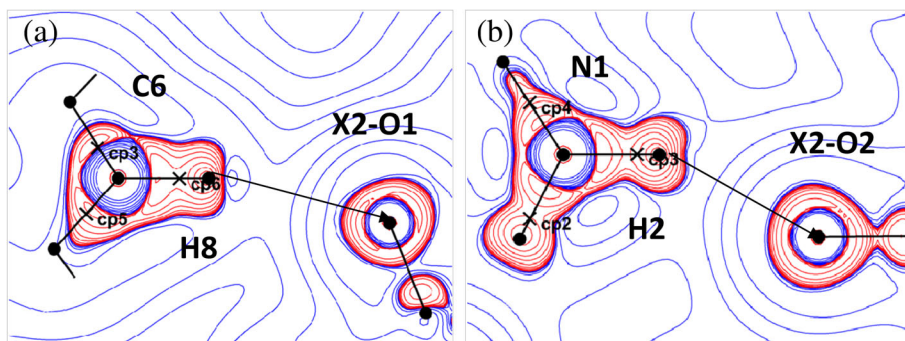
In the crystal, the molecular packing of the 2-amino-4-methylpyridinium 2-(3-methylphenyl)-acetate is stabilized by the N–H...O and C–H...O type of interaction. A topological analysis of the hydrogen bonding interactions was carried out to understand the strength and nature of the interaction as it provides information about molecular recognition.^[44,45] A critical point search was made for

TABLE 5 Topological analysis of hydrogen bonding interactions

D–H...A	R_{ij} (Å)	d_1 (Å)	d_2 (Å)	ρ ($e\text{Å}^{-3}$)	$\nabla^2\rho$ ($e\text{Å}^{-5}$)	λ_1 ($e\text{Å}^{-5}$)	λ_2 ($e\text{Å}^{-5}$)	λ_3 ($e\text{Å}^{-5}$)
H7...O1	1.630	0.563	1.067	0.459	3.36	−2.67	−2.63	8.65
H3...O2	1.850	0.683	1.167	0.258	2.34	−1.17	−1.15	4.66
H2...O2 ⁽ⁱ⁾	1.881	0.713	1.168	0.243	2.37	−1.07	−1.04	4.49
H8...O1 ⁽ⁱⁱ⁾	2.233	0.866	1.367	0.119	1.18	−0.42	−0.42	2.03

Note: (i) x, y, z; (ii) −x, −y, −z.

FIGURE 11 Laplacian map of electron density of 2-amino-4-methylpyridinium 2-(3-methylphenyl) acetate molecule of C6-H8...O1 and N1-H2...O2 hydrogen bonding interactions



all possible intermolecular interactions and the resultant molecular graph is shown in Figure 10. The electron density $\rho_{\text{BCP}}(\mathbf{r})$ and the Laplacian of electron density $\nabla^2\rho_{\text{BCP}}(\mathbf{r})$ values of the corresponding critical points are listed in Table 5. Among the values, notably the $\rho_{\text{BCP}}(\mathbf{r})$ and $\nabla^2\rho_{\text{BCP}}(\mathbf{r})$ values of H7...O1 interaction are found to be much higher than all other bonds, and hence this interaction is found to be the strongest. The contour map of the Laplacian of electron density shows the C6-H8...O1⁽ⁱⁱ⁾ and N1-H2...O2⁽ⁱ⁾ hydrogen bonding interactions between the two neighboring molecules in the crystal (Figure 11). Further, Figure 11b illustrates the alignment of the lone pair lobe of the O2 atom toward the H2 atom and it is clearly visible [symmetry code: (i) x, y, z].

4.8 | Hirshfeld surface and fingerprint analysis

The Hirshfeld surface of the crystal is used to analyze the intermolecular interactions of the molecules in the crystal. It is defined by using the weight function, which is the division of the sum of the promolecule density (spherical atom electron densities) to the sum of the same procrystal density.^[46,47] The Hirshfeld surfaces^[48] and the associated 2D fingerprint plots were plotted using Crystal Explorer 2.1.^[49] Hirshfeld surface enclosing a molecule is given by points where the contribution to the electron density from the molecule chosen is equal to the contribution from all the other molecules. Two distances d_i and d_e were defined for each point on the isosurface. The distance from the point to the nearest nucleus external to the surface is d_e , while d_i is the distance to the nearest nucleus internal to the surface. The normalized contact distance d_{norm} is based on both d_i and d_e and the van der Waal radii of the atom, which helps to recognize the region of intermolecular interactions. The molecular Hirshfeld surfaces of the title molecule were generated using a standard (high) surface resolution with the 3D d_{norm} surfaces mapped over a fixed color scale of -0.556 (red) to 1.272 Å (blue). The surfaces were shown to be

transparent to allow visualization of molecular moiety. The molecular Hirshfeld surface that has been mapped over d_{norm} is shown in Figure 12. The d_{norm} surface was used to identify very close intermolecular interactions. The value of d_{norm} was negative or positive when intermolecular contacts were shorter or longer than van der Waal radii. Red regions on the Hirshfeld surface represent a negative d_{norm} value and a region of close contact, while the blue regions represent a positive d_{norm} value with longer contacts. White region on the surface indicates a d_{norm} value of zero where the distance of contact is exactly equal to the van der Waal separation. The respective acceptor and donor atoms showing strong N1-H2...O2 intermolecular hydrogen bond is indicated as bright red spot on the Hirshfeld surface (Figure 12) and the white region indicates the H...H close contacts. This finding is authenticated by the molecular graph of intermolecular interactions found in Figure 10, and the information present in Table 4 is effectively summarized in these plots.

Fingerprint plots are based on the Hirshfeld surface, which allows the exploration of intermolecular interactions and crystal packing modes in molecular crystals.^[47] The two-dimensional fingerprint plot generated for each

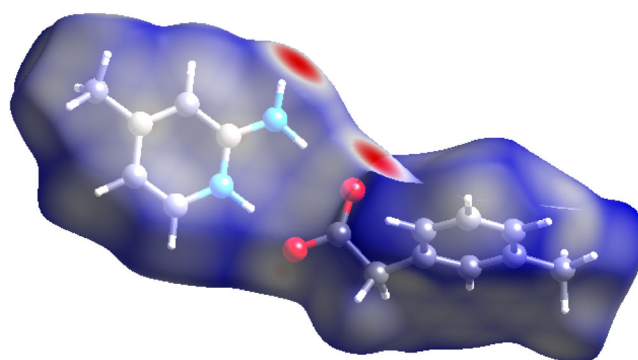


FIGURE 12 Hirshfeld surface of 2-amino-4-methylpyridinium 2-(3-methylphenyl)acetate mapped with d_{norm} . Red and blue regions on the surface show the region of close and long intermolecular contacts

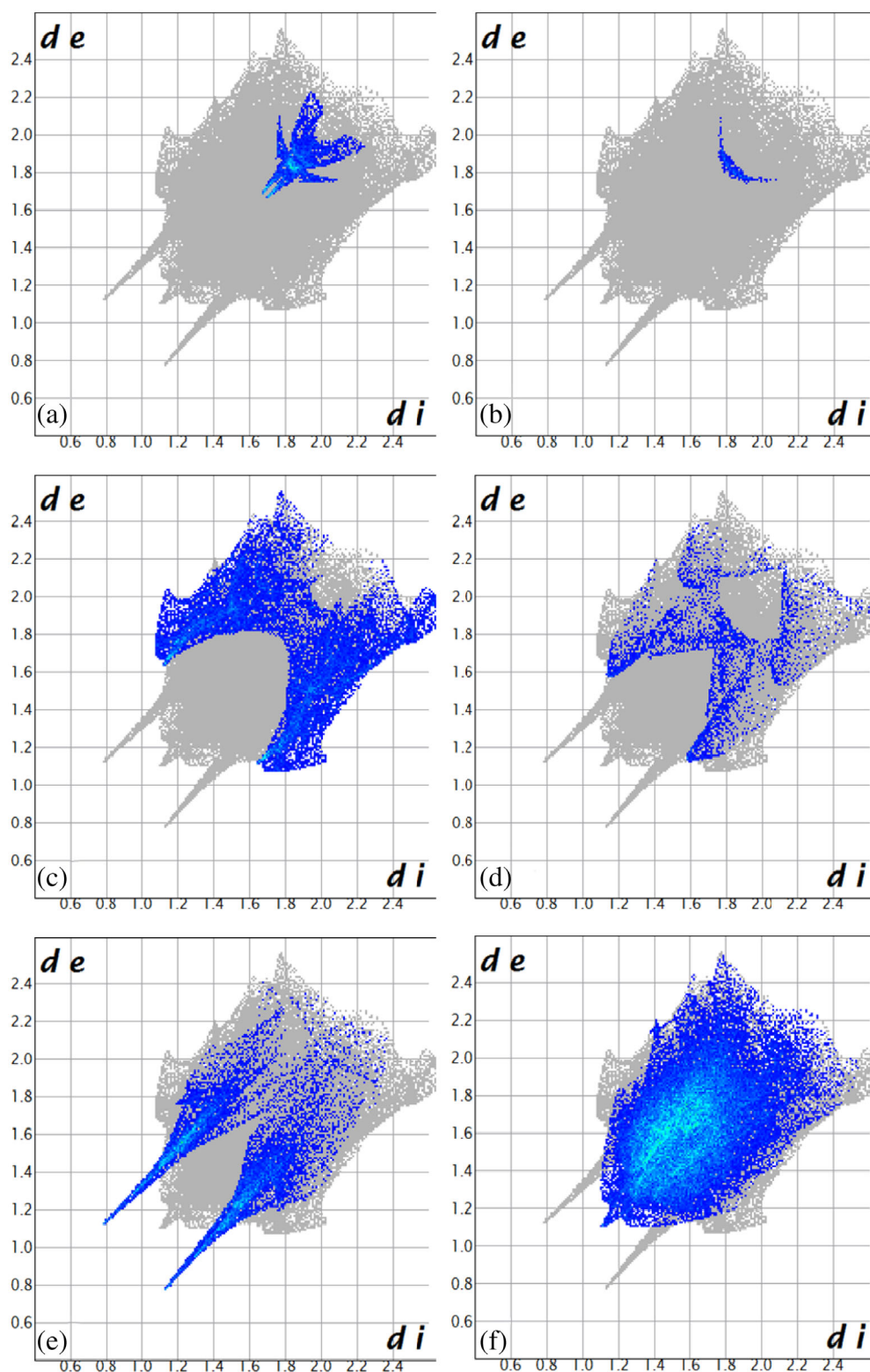
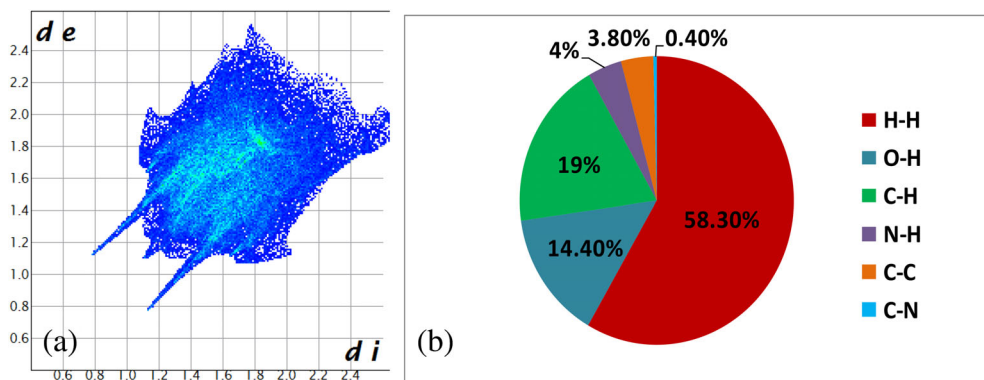


FIGURE 13 Fingerprint plot showing (a) C...C (b) C...N/N...C (c) C...H/H...C (d) N...H (e) O-H and (f) H-H interactions

surface point and the data extracted from which are binned into discrete intervals of d_i and d_e .^[48] The overall two-dimensional fingerprint plot of 2-amino-4-methylpyridinium 2-(3-methylphenyl)-acetate is shown in Figure 14a and those delineated into C...C, C...N/N...C, C...H/H...C, N...H/H...N, O...H/H...O and H...H contacts

are exemplified in Figure 13a-f. These plots quantitatively summarize the nature and type of the intermolecular contacts by illustrating atom_{inside}/atom_{outside} interactions.^[50] The distribution of points in the upper central region of the fingerprint plot of Figure 13a is delineated into C...C contacts and it represents the π - π

FIGURE 14 Fingerprints plot (a) full (b) Percentage of contact contributing to the total Hirshfeld surface area of the 2-amino-4-methylpyridinium 2-(3-methylphenyl)-acetate molecule in the crystal



stacking interactions.^[51] The small contribution from the C...N/N...C contact is found in the upper part of the fingerprint plot and it is identified as the weakest interaction among all other interactions with a contribution of only 0.4%, and hence it has a negligible effect on the packing in the crystal. Similarly, the outer wing-shaped region in the fingerprint plot represents the C...H/H...C contacts with a contribution of 19% to the Hirshfeld surface, while the inner wing-shaped region denotes N...H/H...N interactions with a contribution of 4%. In the fingerprint plot delineated into O...H/H...O contacts, the spikes connected with the C-H...O and N-H...O hydrogen bond interactions are merged within the plot, and the obvious aspect in the plot is a pair of spikes, which corresponds to the most dominant hydrogen bonds. In the title molecule, the contribution from the H...H contacts is observed to be highest toward the Hirshfeld surface with a 58.3% contribution and it appears as a set of diffuse points between the spikes. This shows the packing of the molecules may be further stabilized by the network of H...H interaction.^[52]

5 | CONCLUSIONS

High-resolution X-ray diffraction data were collected for the molecular complex 2-amino-4-methylpyridinium 2-(3-methylphenyl)-acetate at low temperature. The molecular complex was obtained by slow evaporation in m-Tolylacetic acid substituted pyridine molecular complex by utilizing proton transfer. Hansen-Coppens multipole formalism and atoms in molecules theory were used for modeling and analyzing the experimental electron density distribution in the crystal. Bond critical points were found and analyzed in detail to predict the nature and strength of bonds. The crystal structure reveals that the intermolecular N-H...O and C-H...O interactions lead to the formation of three-dimensional network. The bonds N1-H3, N1-H2, and N2-H7 exhibit less Laplacian of electron density compared with other bonds in the

molecule, which reflects that these bonds are involved in hydrogen bonding interactions with the neighboring molecules in the crystal structure of the 2-amino-4-methylpyridinium 2-(3-methylphenyl)-acetate. Among all the intermolecular interactions, the Laplacian of H7...O1 is found to be high and hence N2-H7...O1 is found to be the strongest hydrogen bond. Hirshfeld surface analysis displays all intermolecular interactions within the crystal, and therefore it is ideal for analyzing the crystal packing. The fingerprint plots identify the types of intermolecular interactions and percentage of intermolecular contacts present in the title molecule. In the title molecule, the close contacts are dominated by H...H, O...H/H...O and C...H/H...C contacts and these interactions have clear signatures in the fingerprint plots.

ORCID

Chellam Anzline  <https://orcid.org/0000-0003-0289-3124>
Samuel Israel  <https://orcid.org/0000-0002-6294-351X>

REFERENCES

- [1] W. H. Bragg, *Philos. Trans. R. Soc.* **1915**, 215, 253.
- [2] T. S. Koritsanszky, P. Coppens, *Chem. Rev.* **2001**, 101, 1583.
- [3] R. F. W. Bader, *Atoms in molecules: A quantum theory*, Clarendon Press, Oxford, New York **1995**.
- [4] R. D. Poulsen, A. Bentien, T. Graber, B. B. Iversen, *Acta Crystallogr.* **2004**, A60, 382.
- [5] S. Pillet, M. Souhassou, C. Lecomte, *Acta Crystallogr.* **2004**, A60, 455.
- [6] E. A. Zhurova, V. G. Tsirelson, A. I. Stash, M. V. Yakovlev, A. A. Pinkerton, *J. Phys. Chem. B* **2004**, 108, 20173.
- [7] E. Epinoso, C. Lecomte, E. Molins, S. Veintemillas, A. Cousson, W. Paulus, *Acta Crystallogr.* **1996**, B52, 519.
- [8] J. Garin, J. Orduna, J. I. Ruperez, R. Alcala, B. Villacampa, C. Sanchez, N. Martin, J. L. Segura, M. Gonzalez, *Tetrahedron Lett.* **1998**, 39, 3577.
- [9] S. K. Pal, A. Krishnan, P. K. Das, A. G. Samuelson, *J. Org. Chem.* **2001**, 637-639, 827.
- [10] J. D. Feng, L. K. Yan, Z. M. Su, Y. H. Kan, Y. Q. Lan, Y. Liao, Y. L. Zhu, *Chin. J. Chem.* **2006**, 24, 119.
- [11] M. Gryl, A. Krawczuk-Pantula, K. Stadnicka, *Acta Crystallogr.* **2011**, B67, 144.

- [12] V. R. Hathwar, R. Pal, T. N. Guru Row, *Cryst. Growth Des.* **2010**, *10*(8), 3306.
- [13] R. Thomas, S. Pal, A. Datta, M. K. Marchewka, H. Ratajczak, S. K. Pati, G. U. Kulkarni, *J. Chem. Sci.* **2008**, *120*(6), 613.
- [14] J. R. Sabino, P. Coppens, *Acta Crystallogr.* **2003**, *A59*, 127.
- [15] S. Mebs, J. Henn, B. Dittrich, C. Paulmann, P. Luger, *J. Phys. Chem. A* **2009**, *113*, 8366.
- [16] S. Grabowsky, R. Kalinowski, M. Weber, D. Forster, C. Paulmann, P. Luger, *Acta Crystallogr.* **2009**, *B65*, 488.
- [17] S. Mebs, A. Luth, P. Luger, *Bioorg. Med. Chem.* **2010**, *18*(16), 5965.
- [18] M. Elias, D. Liebschner, J. Koepke, C. Lecomte, B. Guillot, C. Jelsch, E. Chabriere, *BMC. Res. Notes* **2013**, *6*, 308.
- [19] Y. V. Nelyubina, I. V. Glukhov, M. Y. Antipin, K. A. Lyssenko, *Chem. Commun.* **2010**, *46*, 3469.
- [20] I. L. Kirby, M. Brightwell, M. B. Pitak, C. Wilson, S. J. Coles, P. A. Gale, *Phys. Chem. Chem. Phys.* **2014**, *16*, 10943.
- [21] N. K. Hansen, P. Coppens, *Acta Crystallogr.* **1978**, *A34*, 909.
- [22] M. A. Spackman, D. Jayatilaka, *Cryst. Eng. Commun.* **2009**, *11*, 19.
- [23] G. M. Sheldrick, *Acta Crystallogr.* **2015**, *A71*, 3.
- [24] G. M. Sheldrick, *SADABS, Version 2.06, empirical absorption correction program*, University of Gottingen, Germany **2002**.
- [25] C. K. Johnson, *ORTEP, report ORNL-3974*, Oak Ridge National Laboratory, Tennessee, USA **1965**.
- [26] L. J. Farrugia, *J. Appl. Crystallogr.* **1999**, *32*, 837.
- [27] A. L. Spek, *Acta Crystallogr.* **2009**, *D65*, 148.
- [28] L. J. Farrugia, *J. Appl. Crystallogr.* **2012**, *45*, 849.
- [29] B. Guillot, L. Viry, R. Guillot, C. Lecomte, C. Jelsch, *J. Appl. Crystallogr.* **2001**, *34*, 214.
- [30] C. Jelsch, B. Guillot, A. Lagoutte, C. Lecomte, *J. Appl. Crystallogr.* **2005**, *38*, 38.
- [31] E. Clementi, D. L. Raimondi, *J. Chem. Phys.* **1963**, *38*, 2686.
- [32] F. L. Hirshfeld, *Acta Crystallogr.* **1976**, *A32*, 239.
- [33] P. Sivakumar, S. Sudhahar, S. Israel, G. Chakkaravarthi, *IUCrData* **2016**, *1*(x161098), 1.
- [34] P. Sykes, *A guidebook to mechanism in organic chemistry*, 6th ed. John Wiley & sons Inc., New York, NY **1986**.
- [35] C. Anzline, P. Sivakumar, S. Israel, K. Sujatha, *J. Mol. Struct.* **2020**, *1201*, 127208.
- [36] P. Srinivasan, S. N. Asthana, R. B. Pawar, P. Kumaradhas, *Struct. Chem.* **2011**, *22*, 1213.
- [37] A. Stash, V. Tsirelson, *J. Appl. Crystallogr.* **2002**, *35*, 371.
- [38] C. Kalaiarasi, M. S. Pavan, P. Kumaradhas, *Acta Crystallogr.* **2016**, *B72*, 775.
- [39] G. Rajalakshmi, V. R. Hathwar, P. Kumaradhas, *Acta Crystallogr.* **2014**, *B70*, 568.
- [40] F. Benabicha, V. Pichon-Pesme, C. Jelsch, C. Lecomte, A. Khmou, *Acta Crystallogr.* **2000**, *B56*, 155.
- [41] P. Coppens, *X-ray charge density and chemical bonding*, Oxford University Press, Oxford, UK **1997**.
- [42] G. R. Desiraju, *Angew. Chem. Int. Ed. Engl.* **1995**, *34*, 2311.
- [43] Z. Su, P. Coppens, *Acta Crystallogr.* **1992**, *A48*, 188.
- [44] P. Politzer, J. S. Murray, *Theor. Chem. Accounts* **2002**, *108*, 134.
- [45] D. Stalke, *Chem. Eur. J.* **2011**, *17*, 9264.
- [46] M. A. Spackman, P. G. Byrom, *Chem. Phys. Lett.* **1997**, *267*, 215.
- [47] J. J. McKinnon, M. A. Spackman, A. S. Mitchell, *Acta Crystallogr.* **2004**, *B60*, 627.
- [48] M. A. Spackman, J. J. McKinnon, *Cryst. Eng. Commun.* **2002**, *4*, 378.
- [49] S. K. Wolff, D. J. Grimwood, J. J. McKinnon, D. Jayatilaka, M. A. Spackman, *Crystal explorer 2.1*, University of western Australia, Perth **2007**.
- [50] M. Yaman, N. Dege, M. M. Ayoob, A. J. Hussein, M. K. Samad, I. O. Fritsky, *Acta Crystallogr.* **2019**, *E75*, 830.
- [51] J. L. Wardell, M. M. Jotani, E. R. T. Tiekink, *Acta Crystallogr.* **2017**, *E73*, 579.
- [52] S. A. Kohnhorst, S. Saithong, *J. Curr. Sci. Tech.* **2019**, *9*, 77.

How to cite this article: C. Anzline, S. Israel, K. Sujatha, R. A. J. R. Sheeba, *J. Chin. Chem. Soc.* **2022**, *1*. <https://doi.org/10.1002/jccs.202100433>